A Journal of the Gesellschaft Deutscher Chemiker

Angewandte International Edition Chemie

GDCh

www.angewandte.org

Accepted Article

Title: Structural insight into IAPP-derived amyloid inhibitors and their mechanism of action

Authors: Zheng Niu, Elke Prade, Eleni Malideli, Kathleen Hille, Alexander Jussupow, Yonatan Mideksa, Li-Mei Yan, Chen Qian, Markus Fleisch, Ana C. Messias, Riddhiman Sarkar, Michael Sattler, Don C. Lamb, Matthias J. Feige, Carlo Camilloni, Aphrodite Kapurniotu, and Bernd Reif

To be cited as: *Angew. Chem. Int. Ed.* 10.1002/anie.201914559
Angew. Chem. 10.1002/ange.201914559

Link to VoR: http://dx.doi.org/10.1002/anie.201914559
http://dx.doi.org/10.1002/ange.201914559

WILEY-VCH

10.1002/anie.201914559

Structural insight into IAPP-derived amyloid inhibitors and their mechanism of action

Zheng Niu,[a,b] Elke Prade,[b] Eleni Malideli,[c] Kathleen Hille,[c] Alexander Jussupow,[b,d] Yonatan G. Mideksa,[b,d] Li-Mei Yan,[c] Chen Qian,[e] Markus Fleisch,[a,b] Ana C. Messias,[a] Riddhiman Sarkar, [a,b] Michael Sattler,[a,b] Don C. Lamb,[e] Matthias J. Feige,[b,d] Carlo Camilloni,[d,f] Aphrodite Kapurniotu,[c]* and Bernd Reif [a,b]*

December 18, 2019

[a] Helmholtz-Zentrum München (HMGU), Deutsches Forschungszentrum für Gesundheit und Umwelt, Institute of Structural Biology, Ingolstädter Landstr. 1, 85764 Neuherberg, Germany

[b] Technische Universität München (TUM), Munich Center for Integrated Protein Science (CIPS-M) at the Department of Chemistry, Lichtenbergstr. 4, 85747 Garching, Germany

[c] Technische Universität München (TUM), TUM School of Life Sciences, Division of Peptide Biochemistry, Emil-Erlenmeyer-Forum 5, 85354 Freising, Germany

[d] Technische Universität München (TUM), Institute for Advanced Study, Lichtenbergstr. 2a, 85748 Garching, Germany

[e] Ludwig-Maximilians-Universität, Munich, Department of Chemistry, Center for Integrated Protein Science Munich (CIPSM), Nanosystems Initiative Munich (NIM) and Center for Nanoscience (CeNS), Butenandtstr. 5, 81377 München, Germany

[f] Università degli Studi di Milano, Dipartimento di Bioscienze, Via Giovanni Celoria 26, 20133 Milano, Italy

For submission to: *Angewandte Chemie*
To whom correspondence should be addressed:
akapurniotu@wzw.tum.de, reif@tum.de

10.1002/anie.201914559

TOC figure and description for the manuscript

Structural insight into IAPP-derived amyloid inhibitors and their mechanism of action

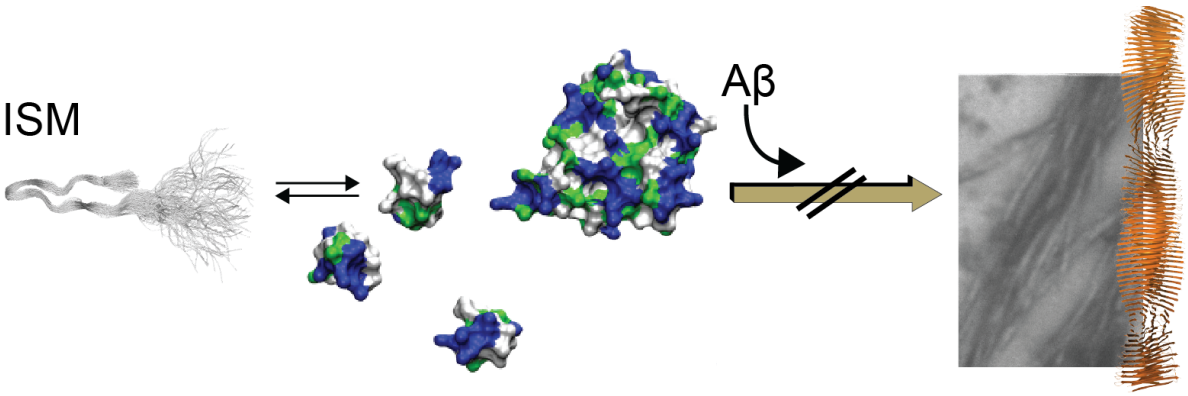

ISM inhibitors are highly dynamic assemblies and exchange between monomeric and high molecular weight states. In both states, the ISM peptide adopts a β-loop like structure, that provides a suitable surface for sequestration of Aβ40 in the colloidal state. ISM inhibitors thus exploit multivalency by self-association to yield high substrate avidity.

10.1002/anie.201914559

Abstract

Designed peptides derived from the IAPP cross-amyloid interaction surface with Aβ (termed interaction surface mimics or ISMs) have been shown to be highly potent inhibitors of Aβ amyloid self-assembly. However, the molecular mechanism of their function is not well understood. Using solution-state and solid-state NMR in combination with ensemble averaged dynamics simulations and other biophysical methods including TEM, fluorescence spectroscopy and microscopy, and DLS, we characterize ISM structural preferences and interactions. We find that the ISM peptide R3-GI is highly dynamic, can adopt a β-like structure and oligomerizes into colloid-like assemblies in a process which is reminiscent of liquid-liquid phase separation (LLPS). Our results suggest that such assemblies yield multivalent surfaces for interactions with Aβ40. Sequestration of substrates into these colloid-like structures provides a mechanistic basis for ISM function and the design of novel potent anti-amyloid molecules.

Keywords: amyloid formation, amyloid inhibitor, peptide, Aβ, solution and MAS solid-state NMR

Introduction

Peptides mimicking the cross-amyloid interactions surface of the type 2 diabetes (T2D) human islet amyloid polypeptide (hIAPP) with the Alzheimer's disease β-amyloid protein Aβ40/42, termed Interaction Surface Mimics (ISMs), have been shown to be nanomolar inhibitors of amyloid self-assembly of Aβ40/42.[1] The molecular mechanism is, however, not well understood. The design of the ISMs was based on the finding that amyloids are generally composed of a β-sheet-turn-β-sheet structural motif and that IAPP uses the same two binding regions for both its amyloid self- and its cross-amyloid hetero-assembly with Aβ40/42.[1a, 2] ISMs were thus derived by linking the two hot segments IAPP(8-18) and IAPP(22-28) in native or N-methylated form to each other via different linkers, mostly tripeptide sequences consisting of identical amino acids; notably, these two segments are highly homologous to segments of the amyloid core of Aβ.[3] High Aβ40/42 anti-amyloidogenic activity was found for 7 out of the 16 studied ISMs with 6 of them containing bulky hydrophobic/aromatic residues (e.g. LLL, III, FFF) in the linker tripeptide and one of them, termed R3-GI, the RRR tripeptide.

It has been recognized recently that liquid-liquid phase separation (LLPS) plays an important role for self-organization of membrane-less cellular organelles.[4] In particular, proteins containing low complexity sequences can form protein-rich droplets.[5] Phase separation is the driving force for the formation of membrane-less cellular organelles like nucleoli, stress granules, P-bodies and other cellular compartments.[6] Similar to stress granules, hydrophobic small molecules undergo LLPS, adopt colloidal structures in aqueous environment,[7] and recruit amyloidogenic proteins into its core in which amyloids adopt an altered structure that prevents amyloid neurotoxicity.[8] The elevated local concentration facilitates interactions with the amyloid.

In this manuscript, we show that R3-GI is highly dynamic, can adopt a β-like structure and oligomerizes into colloid-like assemblies. Our results suggest that formation of such ISM assemblies provides a multivalent surface for interactions with Aβ40, resulting in its sequestration into off-pathway non-toxic aggregates. The suggested mechanism provides a possible mechanistic scenario for the potent amyloid inhibitor function of ISMs.

Design of the studies

Our studies focused on the two ISMs R3-GI and K3-L3-K3-GI for the following reasons (Fig. 1A and Supp. Table S1): (1) R3-GI was used in solution-state NMR studies as the intrinsically low solubility of all ISMs with hydrophobic linkers makes them unsuitable for solution-state NMR; (2) K3-L3-K3-GI was used in MAS solid-state NMR

studies as it is a reasonably soluble and functional analog (Fig. S1) of the sparingly soluble but highly potent L3-GI (LLL in linker) which shows the largest effects in terms of substrate interaction.[1b] A third ISM, the non-inhibitor G3-GI containing the flexible GGG tripeptides as linker, was used as a control peptide.

ISM self-association and exchange between monomeric and oligomeric states

Most of the ISMs self-associate with apparent binding affinities (app. K_d) in the low to mid-nanomolar concentration range.[1b] In the case of R3-GI an app. K_d of 77 nM was determined by titrating synthetic N-terminal fluorescently labeled peptide (Fluos-R3-GI) with R3-GI (Fig. 1A). The high oligomerization propensity of R3-GI was further confirmed by concentration dependent CD studies (Fig. S2D), chemical cross-linking (Fig. 1B) and dynamic light scattering (DLS) (Fig. 1C). In addition, differential interference contrast (DIC) microscopy, fluorescence microscopy and transmission electron microscopy showed that R3-GI aggregation resulted in granule-like, high molecular weight structures (Fig. 1D-F). As expected, R3-GI assemblies within these structures have a significantly retarded translational diffusion coefficient in comparison to particles in isotropic solution (Fig. 1G). Next, we recorded solution-state NMR spectra of R3-GI at a concentration of 1.5 mM (Fig. S2A). At this concentration, peptide self-association should result in aggregates that are too large to be observable by solution-state NMR. Unexpectedly, high intensity and resolution spectra were obtained characteristic for monomeric, random coil peptides. ^{13}C chemical shifts, which are sensitive to secondary structure [9] yielded no indication for formation of neither α-helical nor β-sheet secondary structure elements (Fig. S2C).

In order to resolve the apparent discrepancy between the NMR findings and the results of the other biophysical studies, we performed fluorescence recovery after photobleaching (FRAP) experiments (Fig. 1H). We find that the fluorescence of the granules recovers within seconds, indicating that peptides exchange between the peptide dense phase and bulk solution. In addition, we recorded saturation transfer difference (STD) experiments for R3-GI (Fig. 1I). We observed very intense signals in this experiment, suggesting that R3-GI undergoes chemical exchange between a monomeric random-coil like conformation, and an aggregated state that is too large to be observable for solution-state NMR. In contrast, a non-aggregating monomeric peptide used as a control yielded no STD signals. Notably, a similar behavior has been observed previously for the Alzheimer's disease Aβ peptide which has been shown to exchange between a soluble and an aggregated state.[10] These findings are in agreement with DOSY experiments (Fig. S2E,F). We observe a smaller apparent diffusion coefficient that is consistent with R3-GI undergoing a transition between a

10.1002/anie.201914559

monomeric and an aggregated state. Next, we quantified the amount of R3-GI that in the aggregated state versus solution. For this purpose, we determined the intensities of the fluorescent granules with respect to background (Fig. S3). We find a partitioning coefficient of R3-GI on the order of 2.9, i.e. an approximately 3-fold higher concentration in aggregates in comparison to free solution.

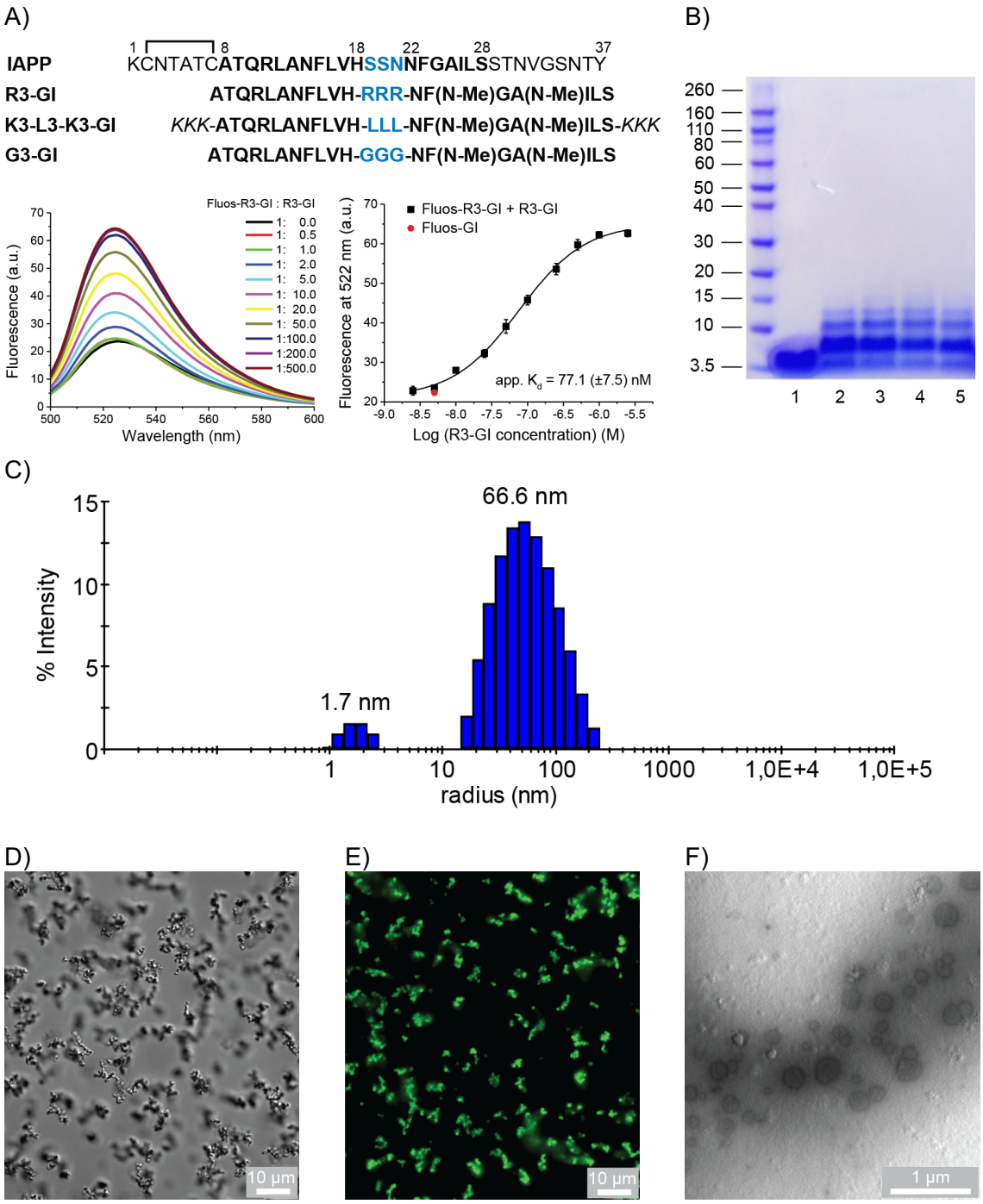

10.1002/anie.201914559

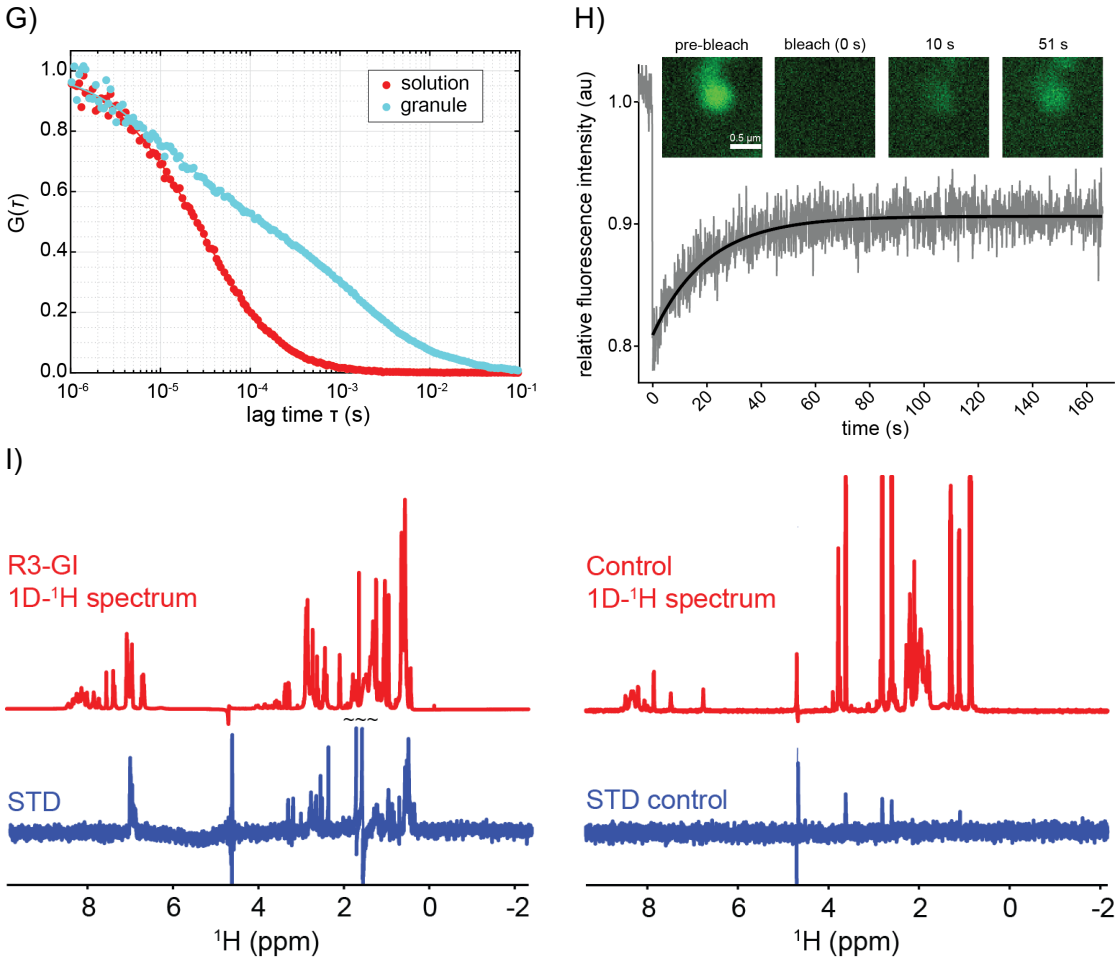

Figure 1. R3-GI self-assembly. *(A) Top, sequences and abbreviations of IAPP and the investigated ISMs. "Hot segments" of the IAPP interaction surface with Aβ40 are shown with black bold letters; residues in the IAPP loop and ISM linker regions are drawn in blue. The L3-GI solubilizing tag "KKK" is shown in italics. Bottom, fluorescence emission spectra of N-terminal fluorescein labeled R3-GI (Fluos-R3-GI) (5 nM) alone and after titration with R3-GI at the indicated molar ratios (pH 7.4). On the right, the binding curve is shown. The estimated app. K_d for R3-GI self-association is 77.1 (±7.5) nM. Data are means (±SEM) from 3 binding curves. (B) R3-GI oligomerization (500 µM) studied by cross-linking with glutaraldehyde and NuPAGE. Lane 1, R3-GI w/o cross-linking; lanes 2-5: R3-GI cross-linked following incubation for 0 h (lane 2), 1 h (lane 3), 24 h (lane 4), and 48 h (lane 5). (C) Dynamic light scattering (DLS) studies of a 50 µM R3-GI in 10 mM sodium phosphate buffer, pH 7.4 (containing 1% v/v HFIP). (D) Differential Interference Contrast (DIC) micrographs of R3-GI (500 µM). The peptide has been imaged immediately after dissolution into 10 mM sodium phosphate buffer, pH 7.4 (containing 1% v/v HFIP) without filtration. The scale bar refers to a length of 10 µm. (E) Microscopic images of Fluos-R3-GI in fluorescence mode. (F) TEM image of R3-GI (500 µM) in 10 mM sodium phosphate buffer, pH 7.4 (containing 1% v/v HFIP). Spherical assemblies are observed with diameters in the range of 200-400 nm. (G) Fluorescence correlation spectroscopy (FCS) of a mixture of 454 µM R3-GI and 454 nM Fluos-R3-GI showing that the translational diffusion inside the R3-GI granules is strongly retarded. (H) Fluorescence recovery after photobleaching (FRAP) of a R3-GI granule. The fast recovery of the fluorescence intensity indicates that the majority of the peptide molecules are exchanging with the bulk solution within seconds. (I) Saturation Transfer Difference (STD) NMR experiments of 1.25 mM R3-GI in 10 mM sodium phosphate buffer, pH 7.4 (containing 1% v/v HFIP and 10% v/v D_2O), show that soluble, monomeric R3-GI undergoes exchange with a high-molecular weight oligomeric R3-GI conformer. As a control, STD spectra of a 60 µM solution of the peptide GVAEPEQDCAVTSGE (Mr = 1.492 kDa) is shown. The control peptide is monomeric under the conditions employed in the experiment.*

10.1002/anie.201914559

NMR structural characterization of R3-GI

Subsequently, we recorded NOESY spectra to assign the resonances of R3-GI (Fig. S2A) and to determine the structure of the peptide. N-methylation increases the population of a cis peptide conformer, and has been suggested to induce a turn structure similar to a proline.[11] As expected, three sets of resonances are observed in the N-methyl region (residues N15-L20). We estimate the populations of the three conformers G17(trans)-I19(trans), G17(cis)-I19(trans), and G17(trans)-I19(cis) to be on the order of 64%, 32% and 4% (Fig. S4). The G17(cis)-I19(cis) conformer is not sufficiently populated to be observable by NMR. Furthermore, we found different sets of resonances at the N-terminal half of the peptide (residues F8-H11, Fig. S5), suggesting that N-methylation assists in turn formation of the monomeric peptide.

The STD NMR and FRAP experiments demonstrate that R3-GI exchanges between a monomeric and an oligomeric form. The experimental NOEs are thus transfer-NOEs[12] containing contributions from the monomeric and the oligomeric state of the peptide. In fact, the observed NOEs are very intense, underlining the exchange contribution to the NOEs. Fig. 2A summarizes the experimental long-range ^{1}H,^{1}H NOE connectivities for R3-GI. The observed contacts are indicative for a structure containing a loop. We investigated further the salt, temperature and pH dependence for loop formation (Fig. S6, S7). Whereas the concentration of salt did not have a significant impact on the intensity of the long-range cross peaks in R3-GI, we found that conditions of low pH significantly increase the intensity of the long-range cross peaks. Similarly, we found that low temperatures increase the fraction of peptides adopting the turn-like structure (Fig. S7). Interestingly, the $(N7\text{-}I19)^{2}$ cross peak intensity seems to correlate with the pKa of the histidine imidazole ring (Fig. S8). We speculate that a lower pH and protonation of the histidine side chain is beneficial for loop formation in the aggregated state. At the same time, low pH has no influence on the population of the two conformers observed in the N-terminal half of the peptide (Fig. S4). We observe long-range NOEs for both conformer 1 (G17(trans)-I19(trans)) and conformer 2 (G17(cis)-I19(trans)) (Fig. 2A). By contrast, the non-inhibitor peptide G3-GI shows only weak long-range NOEs if any, suggesting that the loop-like structure is not adopted for G3-GI (Fig. S9). These results are in good agreement with previous results and support the hypothesis underlying the design of the ISMs.[1b]

10.1002/anie.201914559

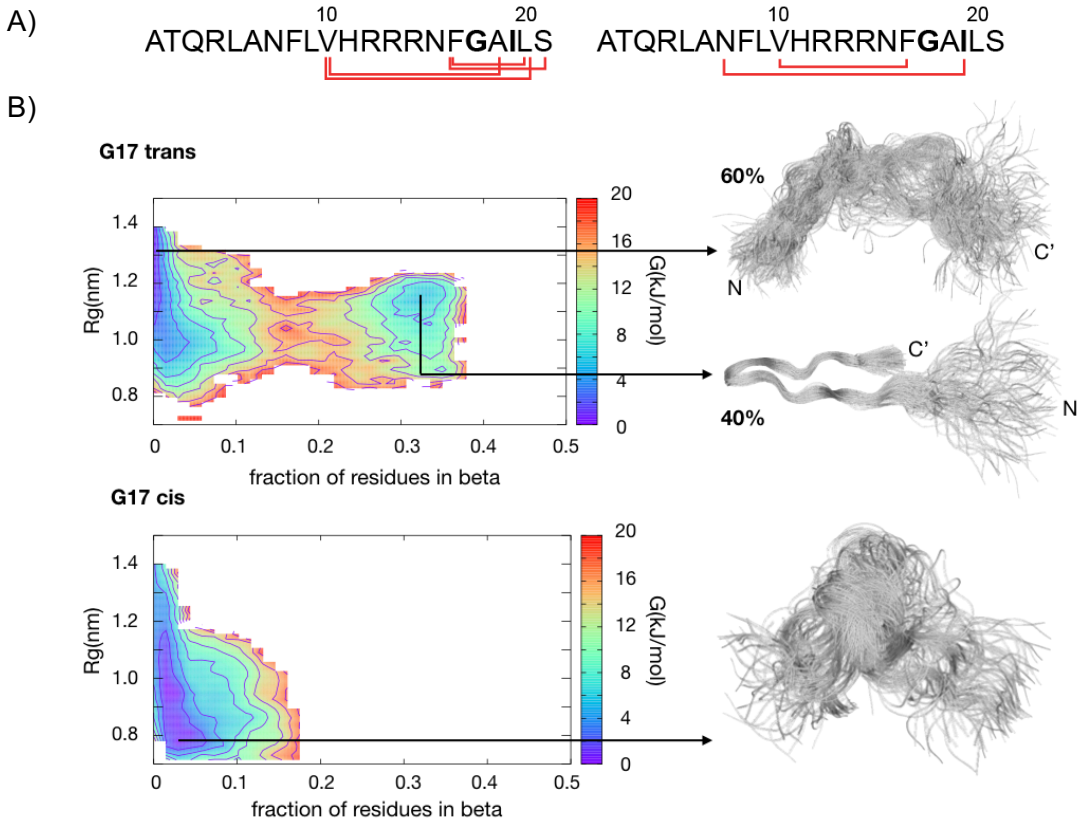

Figure 2. R3-GI NOESY experimental data and molecular modelling of the monomer. *(A) long-distance NOE contacts plotted onto the R3-GI peptide sequence for conformer 1 and 2. (B) Free energy diagram and structural ensembles for R3-GI.*

Conformational ensembles representing the R3-GI conformers 1 and 2 were generated by metadynamic metainference[13] using 221 and 35 inter-residues distance restraints for the first and the second conformer, respectively (Supp. Table S4 and Supp. Table S5). Metadynamic metainference represents an extension of the Inferential Structure Determination approach introduced by Nilges and co-workers for heterogenous systems.[14] Using this method, an optimal coupling of simulations and equilibrium experiments allows to determine the overall ensembles of structures that are compatible with the experimental data, in this case with the NOE derived distances. The calculated ensembles for the two conformers are highly heterogeneous. In fact, a close inspection of the ensembles reveals significant differences. The G17(trans)-I19(trans) ensemble is characterized by an equilibrium between two populations. The first conformer is lacking any secondary structure and adopts a large radius of gyration (~1.3 nm), while the second conformer is characterized by a loop forming a β-like structure involving residues N7-V10 to S21. The free energy for members of the two different populations is rather similar, suggesting that conformers between the two populations may interconvert on a fast time scales (microseconds or less). By contrast, the ensemble for the G17(cis)-I19(trans) conformer does not show any indication for a loop-like structure and is overall more compact with an average radius of gyration of

10.1002/anie.201914559

0.9 nm, reflecting the observed NOE between N7 and I19. The conformational ensembles suggest that the peptide is overall disordered in solution with some preference for a β-like structure in particular for the G17(trans)-I19(trans) conformer.

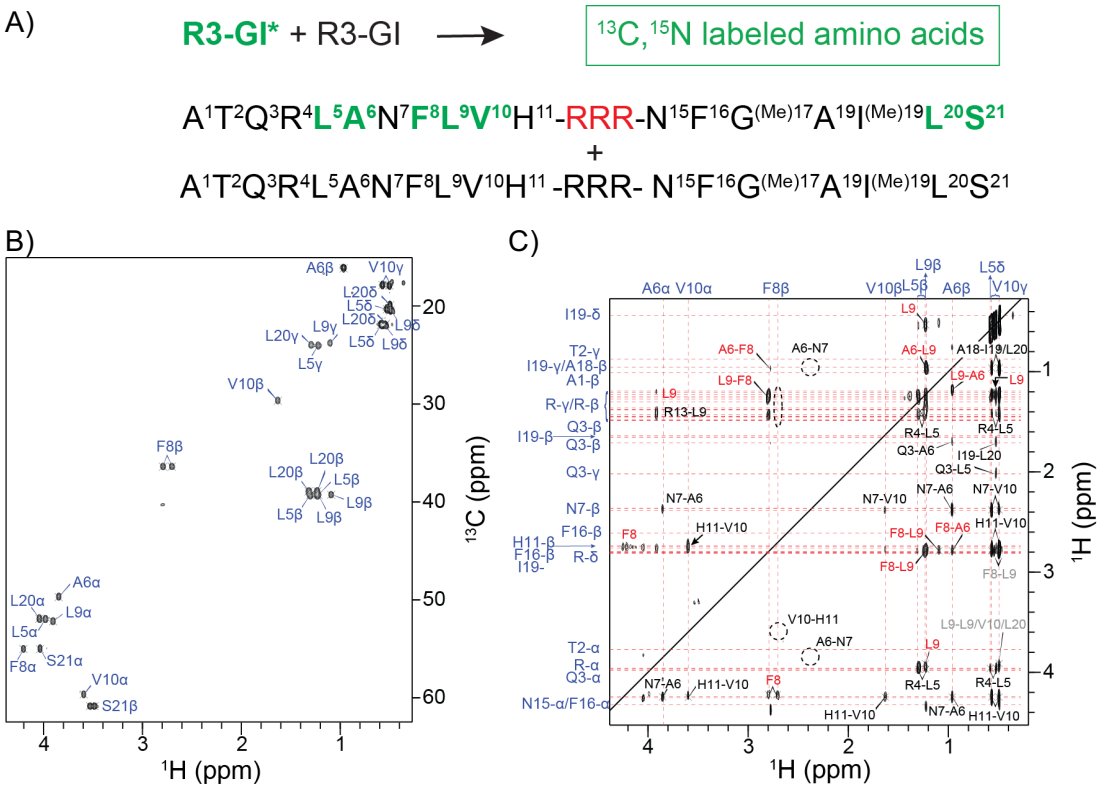

Figure 3. Identification of intermolecular NOEs for R3-GI*. A) Amino acid sequence and labeling scheme for R3-GI. Residues labeled in green are uniformly enriched with ^{13}C and ^{15}N. For the NMR experiment, labeled and non-labeled peptide was mixed in a 1:1 ratio. B) ^{1}H,^{13}C correlation spectrum of R3-GI*. C) ^{1}H (ω_1),^{1}H (ω_3) correlation spectrum extracted from the 3D NOESY experiment. During ω_1, protons were selected which are directly bonded to ^{12}C, whereas ^{13}C bound protons were filtered during ω_3. In addition to trivial sequential connectivities (e.g. H11β-V10α) that appear only on one side of the diagonal, a number of symmetric cross peaks (color coded in red) are observed that are due to intermolecular interactions.*

The NOE intensities cannot easily be disentangled into contributions originating from the monomeric and the oligomeric state of the peptide. In order to probe peptide-peptide contacts in the oligomer, we prepared a mixed sample that contained 50% unlabeled (R3-GI) and 50% labeled peptide (R3-GI*; labeling scheme depicted in Fig. 3). In the experiment, a magnetization filter element is applied during the first evolution period t_1 to remove magnetization of protons that are directly bound to ^{13}C nuclei, following a double half-filter approach.[15] After the NOESY mixing time, ^{13}C bound protons are selected for detection. We found a number of sequential connectivities between labeled and non-labeled residues within one peptide (e.g. H11β-V10α). These cross peaks are detected either above or below the diagonal, indicating that filtering of magnetization works in the intended way. In addition to these intramolecular sequential connectivities, we observe many correlations which yield a symmetric cross

10.1002/anie.201914559

peak both below and above the diagonal (A6β-F8β, A6β-L9β, F8β-L9β, L9β-L9δ). These correlations are due to intermolecular connectivities, as they involve potentially labeled amino acids in both evolution periods.

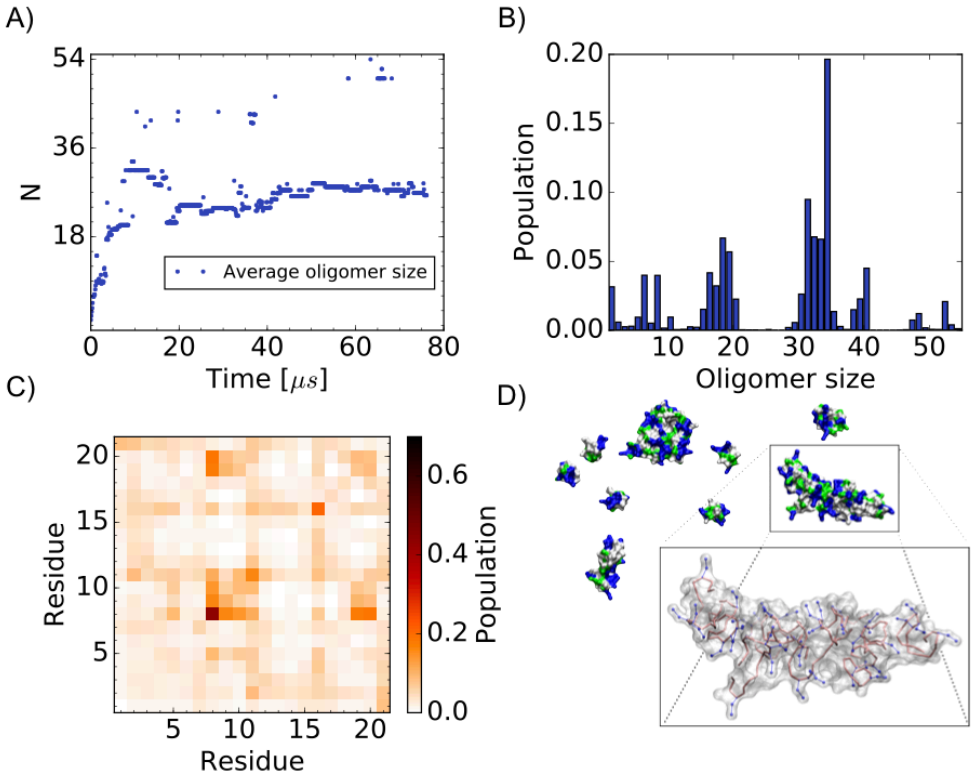

Figure 4. Coarse-grain MD simulations of R3-GI self-assembly. *A) Average oligomer size during the simulation. The simulation was performed using a total of 54 monomers. A value of N=54 would imply that a single oligomer is formed encompassing all the 54 simulated molecules; by contrast, a value of N=1 would indicate that all 54 molecules are monomeric in solution and no oligomers are formed. B) Distribution of the oligomer size over the simulation. C) Intermolecular contact probability map averaged over the simulation. D) Surface representation for a transient oligomeric state (blue for positively charged, red for negatively charged, green for polar and white for hydrophobic side chains). The figure shows an ensemble of monomers and oligomers of different sizes, together with their surface properties. Arginine side chains (in blue) are solvent exposed. The inset shows a single oligomer enlarged, with arginine residues represented in ball and stick mode.*

In order to get more structural insight, we performed MARTINI coarse-grain MD simulations (Fig. 4).[16] 54 monomers were solvated in a cubic box of 22.7 nm lateral length. The structure of the individual monomers was described employing an elastic network centered around a representative G17(trans)-I19(trans) β-turn like conformer. Interestingly, while the molecules self-assembled quickly on the time scale of the simulation (after 10 μs, the average oligomer size was stable between 24 and 30 monomers), the oligomers were overall very dynamic showing a broad distribution of sizes and a significant fraction of free monomers (Fig. 4A, B). Furthermore, monomers can exchange among oligomers on the microsecond time scale in agreement with STD experiments. The monomer-monomer interface is well defined and characterized by

10.1002/anie.201914559

few inter-molecular interactions (Fig. 4C). Arginine side chains are solvent-exposed (Fig. 4D). Intermolecular interactions involve almost only amino acids 7-10. This is in agreement with the experimental intermolecular NOE contacts (Fig. 3C), suggesting that the dynamic oligomer may represent well the macroscopic behavior of R3-GI at a small scale. As a control, five additional simulations were carried out to investigate the role of the linker sequence (Fig. S11). First, the structure of the R3-GI monomer was relaxed by removing the elastic network around the β-like structure, resulting in a more disordered peptide. Interestingly, the overall behavior of the system is robust with respect to this property. The resulting oligomer has a similar dynamics and intermolecular interface, while the average oligomer size is slightly decreased. Further control simulations with and without elastic network were performed for G3-GI and for the peptide $(SG)_{10}S$ with a supposedly totally flexible linker. For G3-GI and $(SG)_{10}S$, the oligomer dynamics disappears. There, monomers self-assemble rapidly into 54-mers. Interestingly, differences can be observed for inter-monomer interactions. While G3-GI retains specific intermolecular interactions very similar to R3-GI, the specific contacts are lost for the $(SG)_{10}S$ peptide. The simulations indicate that both R3-GI and G3-GI can form oligomers with robust intermolecular interactions. The three arginines in the loop of R3-GI induce a β-like structure that may determine the specific dynamic properties of the oligomers that are essential for its inhibitory function.

Substrate interactions

To investigate substrate interactions, we turned to the ISM K3-L3-K3-GI. Upon titration with Aβ40, hetero-complexes precipitated quickly out of solution (Fig. 5A, top). As a control, monomeric Aβ40 was incubated with the non-inhibitor G3-GI and no effects on Aβ40 solubility were observed (Fig. 5A, bottom). At the same time, the chemical shifts of Aβ40 upon titration of the ISM K3-L3-K3-GI are not affected (Fig. 5B). At a 10-fold molar excess of the ISM peptide K3-L3-K3-GI with respect to Aβ40, the 1D-^{1}H solution-state NMR spectrum is almost empty (Fig. 5A, inset), indicating that the two peptides co-precipitated. By contrast, high intensities were observed for the control sample Aβ40·G3-GI (Fig. 5A, inset). Furthermore, fluorescence microscopy showed that K3-L3-K3-GI or R3-GI co-localize with Aβ40 in the aggregates. By contrast, no co-localization with Aβ40 was observed in the case of G3-GI (Fig. 5C).

10.1002/anie.201914559

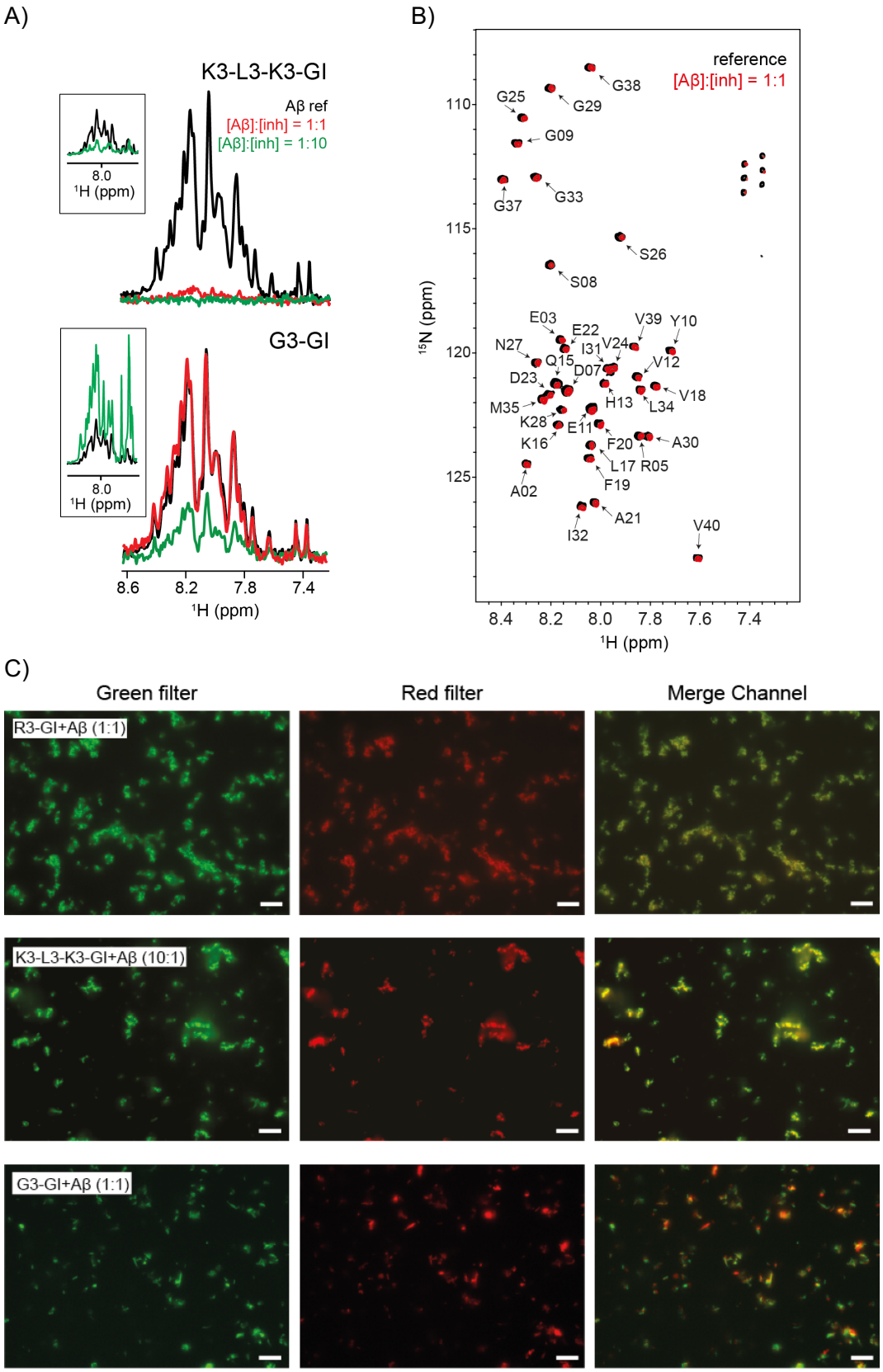

Figure 5: ISM-substrate interactions. *(A) ^{15}N filtered 1D-^{1}H spectra of a 20 μM sample of ^{15}N-labeled Aβ40 in the absence (black) and presence of the ISM inhibitor K3-L3-K3-GI (top), and the non-inhibitor G3-GI (bottom). At a molar ratio of 1:1, only 9 % of Aβ40 remains in solution after addition of K3-L3-K3-GI, whereas the solubility of Aβ40 is almost unaffected upon addition of G3-GI. At a 10x excess of K3-L3-K3-GI, the resonances of Aβ40 disappear quantitatively. At this molar excess, the intensities of Aβ40 are reduced only to ca. 28 % in case G3-GI is titrated*

to Aβ40. The inset shows the 1D-^{1}H spectra of the respective samples. At a molar ratio of 1:10 for Aβ:inhibitor, the spectrum is dominated by the resonances of the inhibitor. The disappearance of all resonances in case of K3-L3-K3-GI indicates that inhibitor and substrate co-precipitate. (B) 2D ^{1}H-^{15}N HSQCs of Aβ40 incubated with K3-L3-K3-GI (red) at a molar ratio of 1:1. The Aβ40 reference spectrum is represented in black. No Aβ40 chemical shift changes are observed after addition of the ISM inhibitor. (C) Comparison of the DIC and fluorescence microscopic images of R3-GI / Aβ40, K3-L3-K3-GI / Aβ40 and G3-GI / Aβ40. Whereas Fluor-647-Aβ40 incubated with either Fluos-R3-GI and Fluos-K3-L3-K3-GI yields a perfect merge, Fluor-647-Aβ40 incubated with Fluos-G3-GI yields a distinct spatial distribution of red and green fluorescent spots, suggesting that G3-GI does not co-localize with Aβ40. Scale bars refer to a length of 10 µm.

The K3-L3-K3-GI induced Aβ40 aggregates were analyzed by TEM and solid-state NMR spectroscopy. TEM indicates the presence of mainly amorphous aggregates while short Aβ40 protofibril-like assemblies were also observed (Fig. 6A,B). At first sight, the ISM induced aggregates appear heterogeneous. However, solid-state NMR experiments yields high-resolution spectra, indicating that the ISM-Aβ40 co-assemblies are homogeneously structured (Fig. 6C). In fact, the spectral resolution obtained for these aggregates is very similar to the resolution obtained for Aβ40 fibrils that are obtained after several rounds of seeding.[17] We performed chemical shift assignments to identify the residues of Aβ40 that are part of the core of the ISM induced aggregates (Table S6). Based on ^{13}Cα and ^{13}Cβ NMR chemical shifts, we predict the β-strand secondary structure elements for K3-L3-K3-GI induced Aβ40 aggregates (Fig. 6D). We find that the same residues as in an Aβ amyloid fibril are immobilized and involved in the β-sheet core.[17] Furthermore, a comparison of the NMR secondary chemical shifts for the two preparations shows a high degree of similarity (Fig. 6E), indicating that the fold of the two aggregates is rather related. In addition, we observe of a TEDOR cross peak involving the carboxyl group of residue D23 and ε-amino group of K28 (Fig. 6F), suggesting the formation of a salt bridge between the two residues. This interaction is a characteristic feature of all Aβ40 fibril structures determined so far,[18] and proofs that also K3-L3-K3-GI induced Aβ40 aggregates adopt a β-arch-like fold upon interaction with a substrate amyloid in the solid-state. Even though the morphology of the K3-L3-K3-GI induced Aβ40 aggregates is rather different in comparison to Aβ40 amyloid fibrils, we conclude that both complexes adopt a similar β-sheet/turn/β-sheet molecular architecture. However, a more detailed structural analysis is necessary to characterize the exact structural features of ISM induced Aβ aggregates.

10.1002/anie.201914559

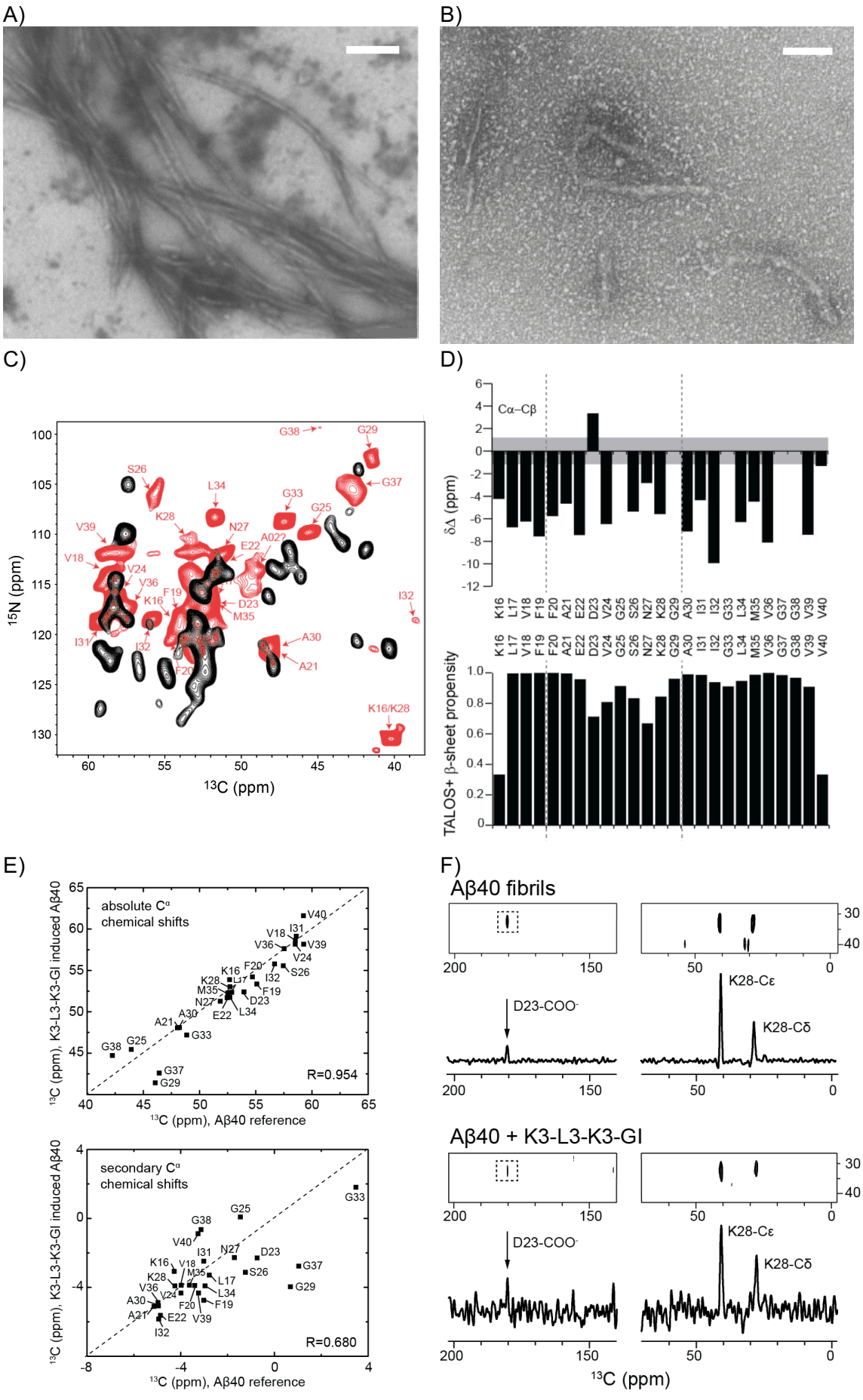

10.1002/anie.201914559

***Figure 6. Structural characterization of K3-L3-K3-GI induced Aβ40 aggregates**. (A, B) Transmission electron microscopy images of Aβ40 in the absence (A) and presence (B) of an equimolar amount of K3-L3-K3-GI. The scale bar denotes a length of 200 nm. (C) 2D $^{13}C,^{15}N$ MAS solid-state NMR correlation spectra obtained for K3-L3-K3-GI induced Aβ40 aggregates (red). To prepare the sample, a 20 μM solution of monomeric Aβ40 was incubated with a 1.23-fold molar excess of K3-L3-K3-GI. For reference, the correlation spectrum obtained for Aβ40 fibrils is represented in black. To prepare the Aβ40 fibril sample, monomeric Aβ40 was grown using 5 % seeds, following the protocol described in Lopez et al.[17] (D) Cα-Cβ chemical shift differences for K3-L3-K3-GI induced Aβ40 aggregates (top). TALOS+[19] predicted secondary structure propensity (bottom). (E) Correlation of the NMR chemical shifts observed for K3L3K3-GI induced Aβ aggregates and Aβ fibrils. On top and bottom, correlations for the absolute and secondary Cα chemical shifts are shown. Secondary Cα chemical shifts indicate differences from random coil chemical shifts. The correlation coefficient is on the order of R=0.954 and R=0.680, respectively. The correlation coefficient is very high, indicating that the conformation in the two different preparations is surprisingly similar. (F) 2D $^{13}C,^{15}N$ TEDOR MAS solid-state NMR spectra for Aβ40 fibrils (top) and K3-L3-K3-GI induced Aβ40 aggregates (bottom). Only the spectral region containing amino side chain nitrogen chemical shifts is shown. For both samples, a long-range correlation peak between Nε of Lys-28 and the carboxylic carbon of Asp-23 is observed, indicating that a salt bridge is formed in the K3-L3-K3-GI induced Aβ40 aggregates. The relative intensity of the long range NH_3-COO^- cross peak appears to be larger in the K3-L3-K3-GI / Aβ40 sample, indicating that this structure is presumably more compact.*

DISCUSSION

We find that the ISM inhibitor R3-GI can adopt a β-like fold in solution. At the same time, we observe supramolecular, granule-like structures by DIC and fluorescence microscopy which suggests that R3-GI may undergo LLPS. STD NMR and FRAP experiments imply that the peptide exchanges between a monomeric and a high molecular weight soluble aggregated state. MAS solid-state NMR experiments show that the β-arch-like architecture of an Aβ40 amyloid fibril with the characteristic salt-bridge between Asp-23 and Lys-28 is preserved in the solid-state in the amyloid-inhibitor complex. R3-GI peptides thus adopt highly dynamic assemblies that provide a suitable surface for sequestration of Aβ40.

Conventional inhibitors, following the classical key-lock or induced fit principle, target specific structural motifs e.g. a deep hydrophobic binding pocket.[20] To be potent, these inhibitors have to be very specific with a high binding affinity. When the binding specificity is reduced, ligands can exploit multivalent interactions to yield avidity. Bacterial toxin inhibitors e.g. are based on multivalent scaffolds.[21] Similarly, most protein–carbohydrate interactions are multivalent to compensate for their low affinities. Multivalency has been employed to trigger signal transduction by inducing receptor clustering,[22] and to design amyloid Aβ inhibitors[23] where small molecule inhibitors have been covalently coupled to chaperones to increase their steric bulk. We suggest that R3-GI and related ISMs exploit multivalency by self-association. The correct spatial arrangement of side chains allows them to efficiently capture Aβ40 and direct it into off-pathway non-toxic aggregates.[24]

10.1002/anie.201914559

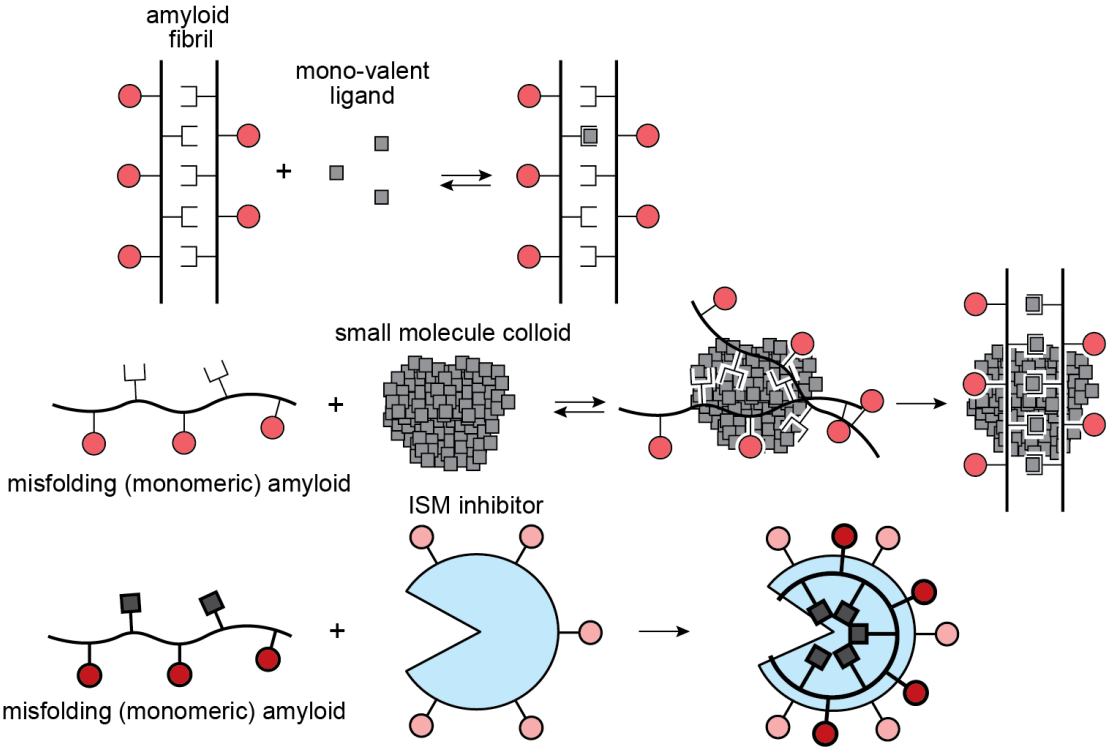

Figure 7. *Schematic representation of different mechanistic pathways of ligand binding to amyloidogenic proteins. (Top) Mono-valent ligands (e.g. small molecules) bind to a specific site in a particular peptide strand. (Center) In colloids, the local concentration of the small molecule concentration is increased, facilitating ligand binding. Amyloid peptides are recruited into the colloid. (Bottom) The IAPP-derived ISM inhibitor R3-GI is suggested to self-assemble and recruit Aβ40 into non-toxic aggregates. Circles and squares represent hydrophilic and hydrophobic side chains, respectively. The inner core of the ISM is represented in light blue to indicate its hydrophobic environment.*

Fig. 7 schematically illustrates different amyloid self-assembly inhibition mechanisms involving classical single-site binding, together with intervention strategies that employ colloid-formation or the here suggested ISM induced LLPS-like process. Single-site binding events are the classical paradigm for a drug-enzyme complex. Due to the low affinity and the lack of deep binding pockets, this class of inhibitors is not very effective for amyloids (Fig. 7, top). Nevertheless, it has been shown that multi-ligand interactions of tramisprosate with monomeric Aβ42 can prevent amyloid oligomer formation.[25] Hydrophobic small molecules can form colloids that resemble in size protein liquid droplets.[7] These small molecule colloids are, however, unspecific inhibitors, as they interact promiscuously with hydrophobic regions of a protein and eventually induce protein unfolding. We have shown previously that NSAIDs (Non-Steroidal Anti-Inflammatory Drugs) such as sulindac sulfide can bind into hydrophobic cavities of amyloid fibrils, and stabilize aggregates.[8, 26] The NSAID accelerates Aβ peptide aggregation by recruiting Aβ peptides into its colloidal core (Fig. 7, center).

Our data suggest that ISMs may act via a similar mechanism: ISMs are active at very low concentrations and make use of multivalent interactions which may dramatically

10.1002/anie.201914559

increase avidity (Fig. 7, bottom). Multivalent interactions between an inhibitor molecule and an amyloid fibril have been exploited by Wall and co-workers[27] who designed an α-helical peptide with a lysine basic side chain to interact with negatively charged residues being exposed on the surface of amyloid structures. These inhibitors are used as imaging reagents and stabilize a fibrillar fold. In contrast, ISMs prevent amyloid formation and redirect Aβ40 into an off-pathway aggregate that lacks cellular toxicity. Importantly, R3-GI self-assembly is likely required but not sufficient for its amyloid inhibitor function. In fact, macroscopic particles are observed in solution for both the non-inhibitor G3-GI and the inhibitor R3-GI in DIC experiments. However, only R3-GI yields long range contacts in NOESY experiments supporting the idea that the specific loop containing structure of R3-GI identified here is essential for its potent inhibitory function.[1b] Notably, Aβ40 in solution exhibits a conformational preference for β-arch like structures as well.[28] Thus, R3-GI and related ISMs may exert their inhibitory function by providing a structural template to which specific, amyloidogenic Aβ40 conformers can adhere.

The highly potent inhibitor function of the ISMs renders them well suited templates for the development of anti-amyloid drugs.[1b, 24b] Our findings provide a molecular basis for understanding their function and should thus assist in the design of novel potent anti-amyloid drugs. In addition, they may contribute to elucidate the mechanism of previously reported self-assembling peptide inhibitors designed to mimic surfaces involved in self- or cross-amyloid interactions, for which the mode of action is so far not understood.[29]

Acknowledgement

We thank Dr. Sam Asami and Dr. Leonidas Emmanouilidis for stimulating discussions. We thank Dr. Karine Farbiarz for synthesis and preliminary studies on K3-L3-K3-GI, Anna Spanopoulou for preliminary DLS studies, and Dr. Erika Andreetto for helpful discussions. We thank Dr. Michaela Aichler and Gabriele Mettenleiter for technical assistance with the EM microscope. We thank the SFB 1035 for financial support (German Research Foundation DFG, Sonderforschungsbereich 1035, projects A11, B06, B07, B11). AJ and CC and MJF acknowledge support of the Technische Universität München, Institute for Advanced Study, funded by the German Excellence Initiative and the European Union Seventh Framework Programme under Grant Agreement No. 291763. DCL acknowledges the support of the Ludwig-Maximilians-Universität, München through the Center for NanoScience (CeNS) and the BioImaging Network (BIN). ZN acknowledges funding of a PhD scholarship by the China Scholarship Council (CSC). YM acknowledges funding of a DAAD PhD scholarship. We gratefully acknowledge the Gauss Centre for Supercomputing e.V. (www.gauss-centre.eu) for funding this project by providing compute time on the GCS Super-computer SuperMUC at the Leibniz Supercomputing Centre (LRZ, www.lrz.de). We are grateful to the Center for Integrated Protein Science Munich (CIPS-M) for financial support. We acknowledge support from the Helmholtz-Gemeinschaft.

References

[1] a) E. Andreetto, L. M. Yan, M. Tatarek-Nossol, A. Velkova, R. Frank, A. Kapurniotu, Angew. Chem. Int. Ed. Engl. 2010, 49, 3081-3085; b) E. Andreetto, E. Malideli, L.-M. Yan, M. Kracklauer, K. Farbiarz, M. Tatarek-Nossol, G. Rammes, E. Prade, T. Neumüller, A. Caporale, A. Spanopoulou, M. Bakou, B. Reif, A. Kapurniotu, Angew. Chem. Int. Ed. 2015, 54, 13095-13100.

[2] D. Eisenberg, M. Jucker, Cell 2012, 148, 1188-1203.

[3] L.-M. Yan, A. Velkova, M. Tatarek-Nossol, E. Andreetto, A. Kapurniotu, Angew. Chem. Int. Edt. 2007, 46, 1246-1252.

[4] D. M. Mitrea, R. W. Kriwacki, Cell Comm. Signal. 2016, 14, 1.

[5] a) A. Molliex, J. Temirov, J. Lee, M. Coughlin, A. P. Kanagaraj, H. J. Kim, T. Mittag, J. P. Taylor, Cell 2015, 163, 123-133; b) Y. Lin, D. S. W. Protter, M. K. Rosen, R. Parker, Mol. Cell 2015, 60, 208-219; c) A. Patel, H. O. Lee, L. Jawerth, S. Maharana, M. Jahnel, M. Y. Hein, S. Stoynov, J. Mahamid, S. Saha, T. M. Franzmann, A. Pozniakovski, I. Poser, N. Maghelli, L. A. Royer, M. Weigert, E. W. Myers, S. Grill, D. Drechsel, A. A. Hyman, S. Alberti, Cell 2015, 162, 1066-1077.

[6] a) C. P. Brangwynne, C. R. Eckmann, D. S. Courson, A. Rybarska, C. Hoege, J. Gharakhani, F. Julicher, A. A. Hyman, Science 2009, 324, 1729-1732; b) C. P.

Brangwynne, T. J. Mitchison, A. A. Hyman, Proc. Natl Acad. Sci. U.S.A. 2011, 108, 4334-4339.
[7] B. Y. Feng, B. H. Toyama, H. Wille, D. W. Colby, S. R. Collins, B. C. H. May, S. B. Prusiner, J. Weissman, B. K. Shoichet, Nature Chem. Biol. 2008, 4, 197-199.
[8] E. Prade, C. Barucker, R. Sarkar, G. Althoff-Ospelt, J. M. Lopez del Amo, S. Hossain, Y. Zhong, G. Multhaup, B. Reif, Biochemistry 2016, 55, 1839–1849.
[9] D. S. Wishart, Sykes, B.D., J. Biomol. NMR 1994, 4, 171-180.
[10] a) S. Narayanan, B. Reif, Biochemistry 2005, 44, 1444-1452; b) N. L. Fawzi, J. F. Ying, D. A. Torchia, G. M. Clore, J. Am. Chem. Soc. 2010, 132, 9948-9951.
[11] a) H. Weisshoff, T. Wieprecht, P. Henklein, C. Frommel, C. Antz, C. Mugge, FEBS Lett. 1996, 387, 201-207; b) B. Laufer, J. Chatterjee, A. O. Frank, H. Kessler, J. Pept. Sci. 2009, 15, 141-146.
[12] F. Ni, Prog. NMR Spectr. 1994, 26, 517-606.
[13] M. Bonomi, C. Camilloni, M. Vendruscolo, Sci. Rep. 2016, 6.
[14] W. Rieping, M. Habeck, M. Nilges, Science 2005, 309, 303-306.
[15] a) G. Wider, C. Weber, R. Traber, H. Widmer, K. Wuthrich, J. Am. Chem. Soc. 1990, 112, 9015-9016; b) M. Ikura, A. Bax, J. Am. Chem. Soc. 1992, 114, 2433-2440; c) J. Cavanagh, W. J. Fairbrother, A. G. Palmer, N. J. Skelton, Protein NMR Spectroscopy: Principles and Practice, Academic Press, San Diego, 1996; d) M. Sattler, J. Schleucher, C. Griesinger, Prog. NMR Spect. 1999, 34, 93-158.
[16] S. J. Marrink, H. J. Risselada, S. Yefimov, D. P. Tieleman, A. H. de Vries, J. Phys. Chem. B 2007, 111, 7812-7824.
[17] J. M. Lopez del Amo, M. Schmidt, U. Fink, M. Dasari, M. Fändrich, B. Reif, Angew. Chem. Int. Ed. 2012, 51, 6136 –6139.
[18] a) R. Tycko, Quart. Rev. Biophys. 2006, 39, 1-55; b) A. K. Paravastu, R. D. Leapman, W.-M. Yau, R. Tycko, Proc. Natl Acad. Sci. U.S.A. 2008, 105, 18349-18354; c) J. X. Lu, W. Qiang, W. M. Yau, C. D. Schwieters, S. C. Meredith, R. Tycko, Cell 2013, 154, 1257-1268.
[19] Y. Shen, F. Delaglio, G. Cornilescu, A. Bax, J. Biomol. NMR 2009, 44, 213-223.
[20] D. E. Koshland, Angew. Chem. Int. Ed. Engl. 1994, 33, 2375-2378.
[21] T. R. Branson, W. B. Turnbull, Chem. Soc. Rev. 2013, 42, 4613-4622.
[22] L. L. Kiessling, J. E. Gestwicki, L. E. Strong, Angew. Chem. Int. Ed. 2006, 45, 2348-2368.
[23] J. E. Gestwicki, G. R. Crabtree, I. A. Graef, Science 2004, 306, 865-869.
[24] a) M. Bakou, K. Hille, M. Kracklauer, A. Spanopoulou, C. V. Frost, E. Malideli, L. M. Yan, A. Caporale, M. Zacharias, A. Kapurniotu, J. Biol. Chem. 2017, 292, 14587-14602; b) A. Spanopoulou, L. Heidrich, H. R. Chen, C. Frost, D. Hrle, E. Malideli, K. Hille, A. Grammatikopoulos, J. Bernhagen, M. Zacharias, G. Rammes, A. Kapurniotu, Angewandte Chemie Int. Ed. 2018, 57, 14503-14508.
[25] P. Kocis, M. Tolar, J. Yu, W. Sinko, S. Ray, K. Blennow, H. Fillit, J. A. Hey, CNS Drugs 2017, 31, 495-509.
[26] E. Prade, H. J. Bittner, R. Sarkar, J. M. Lopez del Amo, G. Althoff-Ospelt, G. Multhaup, P. W. Hildebrand, B. Reif, J. Biol. Chem. 2015, 290, 28737-28745.
[27] J. S. Wall, E. B. Martin, T. Richey, A. C. Stuckey, S. Macy, C. Wooliver, A. Williams, J. S. Foster, P. McWilliams-Koeppen, E. Uberbacher, X. L. Cheng, S. J. Kennel, Molecules 2015, 20, 7657-7682.
[28] a) F. N. Newby, A. De Simone, M. Yagi-Utsumi, X. Salvatella, C. M. Dobson, M. Vendruscolo, Biochemistry 2015, 54, 6876-6886; b) D. Granata, F. Baftizadeh, J. Habchi, C. Galvagnion, A. De Simone, C. Camilloni, A. Laio, M. Vendruscolo, Sci Rep 2015, 5.
[29] a) G. Yamin, P. Ruchala, D. B. Teplow, Biochemistry 2009, 48, 11329-11331; b) P. N. Cheng, C. Liu, M. L. Zhao, D. Eisenberg, J. S. Nowick, Nature Chem. 2012, 4, 927-933; c) M. Richman, S. Wilk, M. Chemerovski, S. K. T. S. Warmlander, A. Wahlstrom, A. Graslund, S. Rahimipour, J. Am. Chem. Soc. 2013, 135, 3474-

10.1002/anie.201914559

3484; d) K. M. Pate, B. J. Kim, E. V. Shusta, R. M. Murphy, Chemmedchem 2018, 13, 968-979.